© 2020. Published by The Company of Biologists Ltd | Journal of Cell Science (2020) 133, jcs252254. doi:10.1242/jcs.252254

TOOLS AND RESOURCES

Trackosome: a computational toolbox to study the spatiotemporal dynamics of centrosomes, nuclear envelope and cellular membrane

Domingos Castro[1], Vanessa Nunes[1], Joana T. Lima[1], Jorge G. Ferreira[1,2,*,‡] and Paulo Aguiar[1,*,‡]

ABSTRACT

During the initial stages of mitosis, multiple mechanisms drive centrosome separation and positioning. How they are coordinated to promote centrosome migration to opposite sides of the nucleus remains unclear. Here, we present Trackosome, an open-source image analysis software for tracking centrosomes and reconstructing nuclear and cellular membranes, based on volumetric live-imaging data. The toolbox runs in MATLAB and provides a graphical user interface for easy access to the tracking and analysis algorithms. It provides detailed quantification of the spatiotemporal relationships between centrosomes, nuclear envelope and cellular membrane, and can also be used to measure the dynamic fluctuations of the nuclear envelope. These fluctuations are important because they are related to the mechanical forces exerted on the nucleus by its adjacent cytoskeletal structures. Unlike previous algorithms based on circular or elliptical approximations, Trackosome measures membrane movement in a model-free condition, making it viable for irregularly shaped nuclei. Using Trackosome, we demonstrate significant correlations between the movements of the centrosomes, and identify specific oscillation modes of the nuclear envelope. Overall, Trackosome is a powerful tool that can be used to help unravel new elements in the spatiotemporal dynamics of subcellular structures.

KEY WORDS: Tracking subcellular structures, Centrosome movement correlations, Membrane reconstruction, Nuclear envelope fluctuations, Mitosis, Free and open-source software

INTRODUCTION

Mitosis is a highly regulated stage of the cell cycle in which multiple subcellular structures take part in a complex chain of events that culminate in chromosome segregation. As cells prepare to enter mitosis, adhesion complexes disassemble (Dao et al., 2009) and the cytoskeleton reorganizes (Matthews et al., 2012; Mchedlishvili et al., 2018). At the same time, duplicated centrosomes need to migrate along the nuclear envelope (NE) so that a bipolar spindle can form (Tanenbaum and Medema, 2010). This process requires the activity of multiple players, such as microtubule-associated motors kinesin-5 (Whitehead et al., 1996) and dynein (Raaijmakers et al., 2012), but also actin (Cao et al., 2010) and myosin II (Rosenblatt et al., 2004). How the dynamic changes in all these events are coordinated in space and time to ensure efficient centrosome separation and spindle assembly remains unknown.

Recent advances in live-cell imaging and image analysis techniques have made it possible to access the subcellular environment and quantitatively examine its underlying mechanisms (Gerlich et al., 2001; Otsuka et al., 2018). Commercial imaging software such as Imaris and Metamorph are equipped with automatic particle tracking functions, which have been used to track centrosome pairs in three dimensions (Collins et al., 2014; De Simone et al., 2016; Yamashita et al., 2015). The open-source freeware ImageJ (Eliceiri et al., 2012) with its particle-tracking plugin Trackmate (Tinevez et al., 2017) has also been used for centrosome tracking in several studies (Boudreau et al., 2019; Mahen, 2018; Stiff et al., 2020). However, these generic tracking tools are not fine-tuned for the appearance and motion dynamics of centrosome pairs, which limits their tracking performance and often requires exhaustive parameter optimization, particularly when high-quality videos are not available. Moreover, when studying the dynamics of spindle formation, it is often necessary to analyze centrosome movement in reference to the cellular and nuclear membrane (and, therefore, in a non-canonical coordinate system). To the best of our knowledge, the available computational tools do not directly allow analysis of the coordinated changes between different structures in specific subcellular frames of reference (such as the nuclear membrane).

The NE also exhibits rich spatiotemporal dynamics, displaying measurable oscillations that correlate with the forces exerted by chromatin, nuclear lamina and the cytoskeleton (Chu et al., 2017; Schreiner et al., 2015; Stephens et al., 2017) and strongly influence nuclear functions (Jahed and Mofrad, 2019; Stephens et al., 2019). One way to study this complex interplay between cytoskeletal forces imposed on the nucleus and the resistive forces triggered by chromatin and nuclear lamina is by measuring the dynamics of NE membrane fluctuations (Chu et al., 2017; Hampoelz et al., 2011; Schreiner et al., 2015), which allow the distinction between thermally driven and active fluctuations (Chu et al., 2017). Importantly, during mitotic entry, chromosomes condense (Antonin and Neumann, 2016) and the nuclear lamina disassembles (Georgatos et al., 1997). How these events affect the pattern of NE oscillations and impact other aspects of early spindle assembly remains to be determined. Current methods used to calculate NE fluctuations were developed under the assumption that each point of the membrane oscillates radially around its time-averaged position (Almonacid et al., 2019; Blanchoud et al., 2010; Caragine et al., 2018; Chu et al., 2017; Schreiner et al., 2015). However, describing the membrane deformations as a radial displacement is a coarse approximation that can lead to erroneous results. Also, to the best of our knowledge, there are no available toolboxes for calculating these membrane fluctuations.

Driven by these computational limitations and the need to better characterize the crosstalk between subcellular structures during mitotic entry, we developed the open-source software Trackosome. This novel computational tool enables a quantitative analysis of the

[1]i3S - Instituto de Investigação e Inovação em Saúde, Universidade do Porto, 4200-135 Porto, Portugal. [2]Departamento de Biomedicina, Faculdade de Medicina, Universidade do Porto, 4200-450 Porto, Portugal.
*These authors contributed equally to this work

‡Authors for correspondence (jferreir@ibmc.up.pt; pauloaguiar@ineb.up.pt)

V.N., 0000-0001-8568-4269; J.T.L., 0000-0002-2327-8852; J.G.F., 0000-0001-6802-3696; P.A., 0000-0003-4164-5713

Handling Editor: David Stephens
Received 26 July 2020; Accepted 2 November 2020

Journal of Cell Science (2020) 133, jcs252254. doi:10.1242/jcs.252254

spatiotemporal dynamics of three cellular components: centrosomes, NE and cellular membrane. Trackosome relies on live-cell imaging datasets, where the structures of interest are independently tagged. The tool has two modules: (1) the Centrosome Dynamics module, used for tracking the centrosomes (or other subcellular organelles) in 3D and study their spatiotemporal relations with the nucleus and cell membrane; (2) the Nuclear Envelope Fluctuations module, used to reconstruct, measure and analyze the dynamic fluctuations of the nuclear membrane (or other membranes) in 2D. The accurate 3D reconstruction of the centrosome trajectories relative to the nucleus and cell membranes (in ellipsoidal coordinates) allowed us to unravel and quantify a significant correlation between centrosome trajectories that has not previously been characterized. In addition, the Nuclear Envelope Fluctuations module allowed us to observe and quantify distinct patterns of membrane oscillations in 2D in different stages of the cell cycle.

Trackosome is made publically available (open-source) as a platform-independent MATLAB toolbox and can be downloaded from https://github.com/Trackosome.

RESULTS

Dynamics of cellular reorganization during early spindle assembly

Tracking and trajectory analysis of centrosomes is performed in the Trackosome toolbox through the Centrosome Dynamics module. This module has a graphical user interface (Fig. 1A; Fig. S1, Movies 1-3) that provides useful feedback about the automatic tracking status, and allows manual or semi-automatic corrections whenever needed. The accuracy of the tracking algorithm was tested and validated in synthetic data, created with imposed controlled conditions. The videos generated had two centrosome-like objects moving in 3D with biologically realistic dynamics (coordinates taken from real centrosome trajectories), in a noisy environment. We set three levels of tracking difficulty by varying the signal-to-noise ratio (Fig. 1B). The coordinates obtained by the Trackosome algorithm were then compared with the original coordinates used to create the videos (Fig. 1C). Our tool was able to track the centrosomes with high fidelity even in highly noisy environments (signal-to-noise ratio of 0.7) where the particles were almost indistinguishable from the background. For all videos analyzed, the root mean squared error associated with the tracking (Fig. 1C) was at the subpixel level (1 pixel=0.189 µm).

We then recorded cells seeded on line micropatterns to normalize cell and nuclear shape (Versaevel et al., 2012). Note, however, that Trackosome does not require cells to be seeded in such micropatterns and can be used in unconstrained conditions (Fig. S3A-D). Taking advantage of the precision provided by Trackosome, we quantified specific spatiotemporal relations between three cellular structures during mitotic entry, namely centrosome pair, nuclear membrane and cell membrane. We chose this stage of the cell cycle as it involves extensive dynamic reorganization of the entire cell (Champion et al., 2017), providing a good benchmark to test the ability of Trackosome to detect these dynamic changes. Here, Trackosome was able to reconstruct in 3D the surfaces of the membranes, together with the trajectories of centrosomes (Fig. 2A,B). Based on their relative positions, the software was able to output different quantitative metrics, such as the distance and angles between centrosomes (Fig. 2C,D), the eccentricity of the nuclear and cellular membranes (Fig. 2E) and the angles between the major axes of the nucleus, cell and centrosomes (Fig. 2F). These metrics describe the intracellular reorganization that occurs as cells enter mitosis, such as movement of the centrosomes to opposite sides of the nucleus (Fig. 2B-D) and nucleus-centrosome axis reorientation (Fig. 2B,F), which we previously described (Nunes et al., 2020).

Centrosome trajectories are not independent

HeLa or U2OS cells labeled with histone H2B-GFP/α-tubulin-RFP/SiR-actin or EB3-GFP/Lifeact-mCherry/SiR-DNA, respectively, were tracked until nuclear envelope breakdown (NEB). During this stage, nuclear shape remained approximately constant and correlated with the labeled chromatin, allowing us to define the median nucleus membrane (Fig. 2G, grey mask) based on the 3D reconstructions of the NE. The centrosomes, on the other hand, exhibited complex trajectories that resembled a search or adaptive path around the nucleus (Fig. 2G). For this reason, to infer the coordination of movement between centrosomes, their trajectories were analyzed using the nucleus as a reference. An ellipsoid was fitted to the median nuclear membrane, setting the frame of reference for the new coordinate system (Fig. S3F-H). Each point of the centrosome trajectory was defined by a latitude ϕ, longitude λ

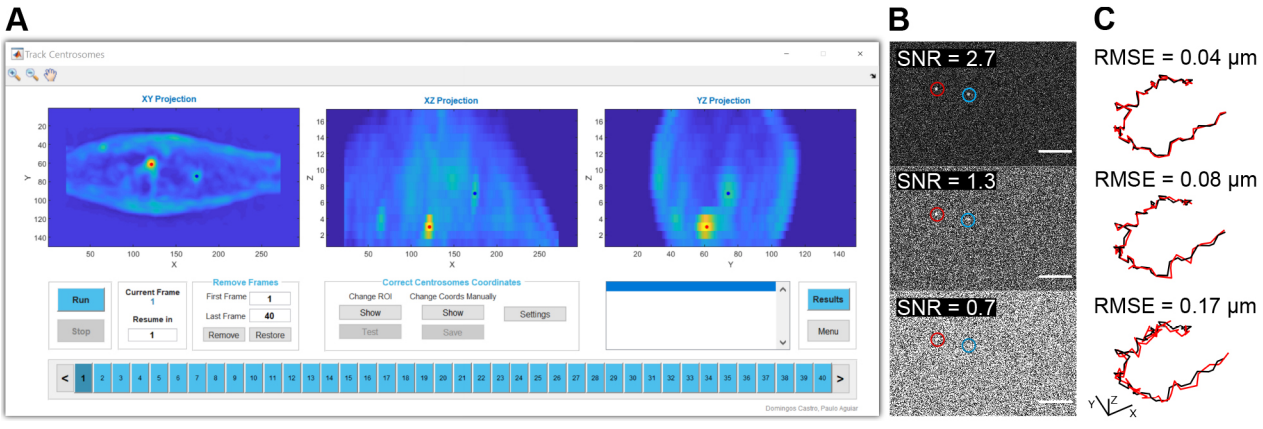

Fig. 1. Evaluation of centrosome tracking. (A) User interface for centrosome tracking showing the XY, XZ and YZ maximum projections for a video of a mitotic cell with the corresponding automatically identified centrosome positions (red and blue dots). (B) Frame extracted from the three synthetic videos with varying levels of signal-to-noise ratio (SNR). Centrosomes are inside the red and blue circles. (C) Ground-truth trajectory (black) and trajectory obtained by Trackosome (red) for the centrosome on the left in B (red circle), and associated root mean square of the error (RMSE) obtained for both centrosomes. Scale bars: 10 µm (B), 1 µm (C).

Journal of Cell Science (2020) 133, jcs252254. doi:10.1242/jcs.252254

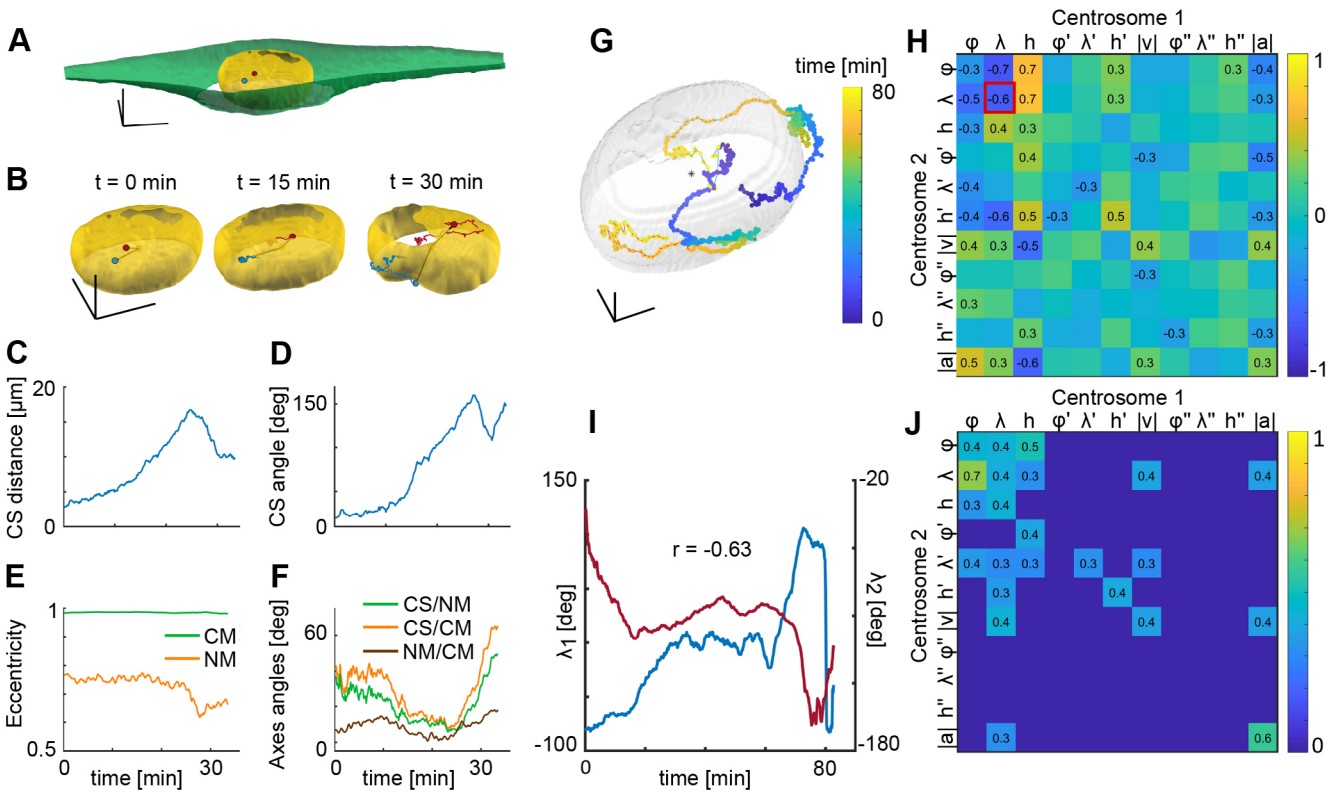

Fig. 2. Spatiotemporal relations between cellular structures during early mitosis. (A-F) Example of Trackosome outputs for a representative cell in mitosis. (A) 3D reconstruction of the cellular membrane (green), nuclear envelope (yellow) and centrosomes (red and blue dots). (B) Nuclear membrane and centrosomes at three distinct time stamps. The centrosome trajectories (red and blue lines) highlight their migration to opposite poles of the nucleus, followed by progressive nuclear deformation. (C) Distance between centrosomes (CS) over time. The distance increases gradually during centrosome migration and decreases once the centrosomes start compressing the nucleus. (D) Angles formed between the centrosomes and the nucleus centroid over time. Note how the decrease in distance between the centrosomes (C) occurs after centrosomes are on opposite sides of the nucleus, corresponding to the highest value for the centrosome-nucleus angle. (E) Eccentricity of the cellular (CM, green) and nuclear (NM, orange) membranes evidencing that, although the cellular membrane remains morphologically stable, the nuclear membrane undergoes conformational changes after the centrosomes start deforming the nucleus. (F) Angles formed between the centrosome axis and the nucleus major axis (orange), centrosome axis and the cell major axis (green), and the nucleus major axis and the cell major axis (brown). The centrosome pair progressively moves towards a disposition perpendicular to the major axis of the nucleus and cell. (G-J) Trajectories of centrosome pairs are spatiotemporally correlated. (G) Centrosome positions across time (color-coded for elapsed time) surrounding the nucleus (gray). (H) Correlation matrix of the movement components (in ellipsoidal coordinates) for the trajectories shown in G. (I) Example of the correlated features highlighted in H (red square), corresponding to the longitude components of both centrosomes, which suggests a potential mechanical coupling between both structures. (J) Median of the absolute correlation matrices obtained from videos of different cells (n=5), thresholded at 0.3 for visualization purposes, showing consistent correlations between centrosome trajectories across different cells. Scale bars: 10 µm (A,B), 5 µm (G).

and height h; the respective ellipsoidal velocities ϕ', λ', h' and velocity norm $|v|$; and the ellipsoidal accelerations ϕ'', λ'', h'' and acceleration norm $|a|$. We calculated the correlation matrix of these features for each centrosome pair (Fig. 2H), revealing which components were temporally correlated between the two trajectories. Our results indicate a considerable degree of similarity and synchrony among trajectory pairs (Fig. 2I), with correlation values as high as 0.7, in contrast to a previous report (Waters et al., 1993). By calculating the median of the absolute correlation matrices obtained, we produced a map of the most consistent correlations (Fig. 2J). Interestingly, the positions of the centrosomes, ϕ, λ, h, and the acceleration norm $|a|$, showed significant correlations. The latter is particularly relevant because the acceleration of a particle reflects the force applied to it, suggesting a synchronous variation of the forces applied to both centrosomes, probably driven by kinesin-5 (Whitehead et al., 1996) or dynein (Raaijmakers et al., 2012). It is worth emphasizing that if the movement of centrosomes had been described in Cartesian coordinates (i.e. ignoring the nuclear surface constraint), the observed correlations would not be evident.

Dynamics of nuclear envelope fluctuations driving mitotic entry

The dynamic morphology of the NE was analyzed using the Membrane Fluctuations module of Trackosome (Fig. S2; Movies 4 and 5). The membrane oscillations were determined by calculating the orthogonal displacement of each point of the membrane with respect to its medial position (Fig. S3I,J). Our new method does not rely on prior assumptions regarding the nucleus shape. We believe that this approach leads to a more realistic description of the membrane displacements than the radial displacement approximations (with respect to the centroid of the membrane) usually described in the literature (Almonacid et al., 2019; Blanchoud et al., 2010; Caragine et al., 2018; Chu et al., 2017; Schreiner et al., 2015). The radial displacements are particularly flawed for an irregularly shaped nucleus with wide fluctuations (Fig. 3A), which generally limits its use to cells in interphase. Here, we were able to quantify and compare the nuclear deformations for cells in interphase and early mitosis.

As before, we recorded cells seeded on line micropatterns. From our analysis, it is possible to confirm that cells in interphase present subtle but measurable nuclear membrane movements. As a negative

Journal of Cell Science (2020) 133, jcs252254. doi:10.1242/jcs.252254

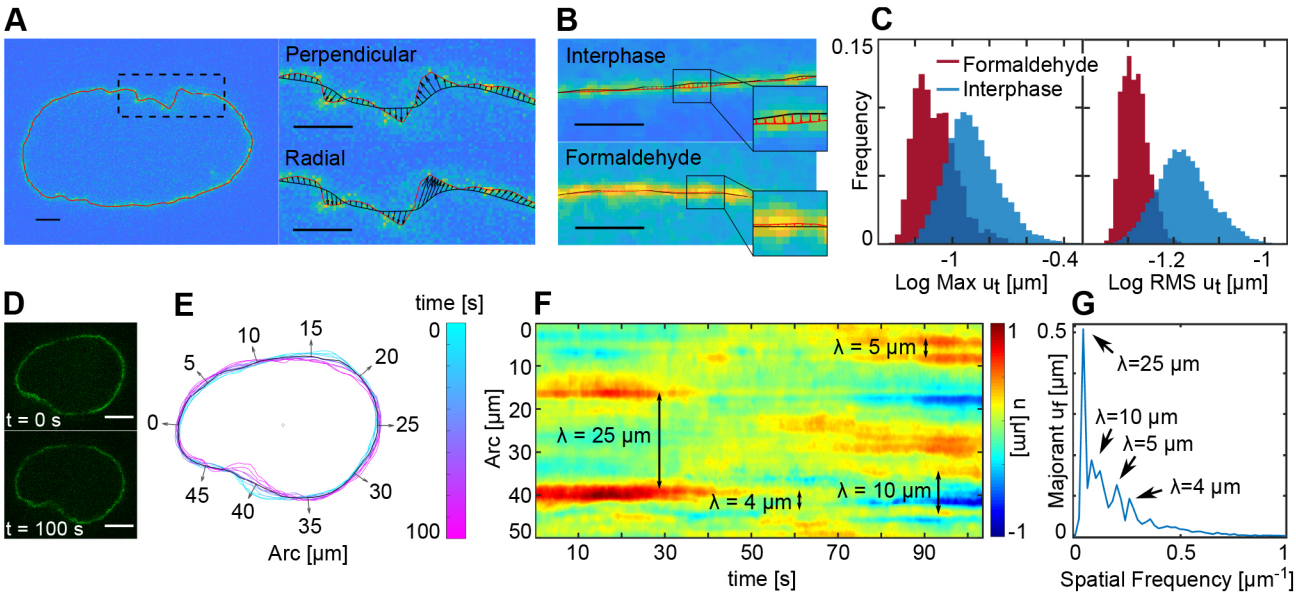

Fig. 3. Nuclear membrane fluctuations captured with Trackosome. (A-C) The perpendicular membrane displacements measured with Trackosome are sensitive to subtle membrane movements. (A) Membrane segmentation (red) of a representative nucleus in prophase (left) and a detailed view of the upper region of the membrane (right) illustrating the difference between defining the fluctuations (black vectors) as perpendicular (top right) or radial (bottom right) movements of the current membrane (red) around the median membrane (black). For the radial displacements, the centroid of the median membrane is used as origin. Perpendicular displacements offer a more realistic description of the membrane movement around its basal position. (B) Representative examples of the nuclear membrane fluctuations (red vectors) of a cell in interphase (top) and a cell fixed in formaldehyde (bottom). The small fluctuations measured for the cell in interphase are clearly larger than those obtained for the fixed cell, suggesting that they are the result of subtle membrane movements. (C) Distributions of the maximum fluctuation per frame, Max u_t (left), and the root mean square (RMS) of the fluctuation per frame, RMS u_t (right), for cells in interphase (44 cells with approximately 600 frames each) and in formaldehyde (4 cells with approximately 500 frames each). With logarithmic scales, the distributions are approximately Gaussian and easily distinguishable. (D-G) Typical nuclear fluctuations results obtained with Trackosome for a cell in prophase. (D) Two frames of the original video. (E) Centered nucleus membrane extracted from the video in D at different time stamps (colored scale), with vectors (gray) indicating the arc in micrometers around the median membrane (black), pointing in the direction along which the fluctuations are calculated. (F) Map of the fluctuations amplitude, u, obtained for all the frames. The y-axis corresponds to the arc around the median membrane, marked by the vectors in E. (G) Majorant of frequency-dependent fluctuations, u_f, obtained by finding the maximum amplitude of the spatial Fourier transform (FT) for each frequency across frames. This FT curve shows the maximum fluctuation amplitude of each wavelength; thus, its peaks reveal the amplitude and wavelength of the most significant curvatures of the nuclear envelope, evidenced both in E and F. Scale bars: 2 μm (A), 2 μm (B), 5 μm (D).

control, fluctuation measurements were made for interphase cells fixed with formaldehyde, which showed a significant decrease in undulations upon fixation (Fig. 3B,C).

During mitotic entry, chromosomes condense (Antonin and Neumann, 2016) and the nuclear lamina disassembles (Georgatos et al., 1997). Whether these events change nuclear behavior remains to be determined. We analyzed the nuclear membrane fluctuations of cells using Trackosome (Fig. 3D-G). After segmenting and registering (centering on centroid) the NE (Fig. 3E), the fluctuations (u) of each frame were calculated assuming normal displacements (Fig. 3A, top). The values obtained were concatenated frame-by-frame and filtered in time and space with a 2D Gaussian kernel. The resulting fluctuations map reveals how the envelope curvatures are dominated by specific wavelengths (Fig. 3F). These wavelengths are determined by calculating the spatial Fourier transform (FT) of the fluctuations, u_f, for each frame and then obtaining the maximum magnitude of each wavelength across frames (Fig. 3G). Calculating the majorant for each frequency component u_f has the advantage of highlighting the most well-defined spatial frequencies, even if they occur for a limited number of frames. On the other hand, averaging the FT curves of all frames would attenuate these components, and the magnitude of the final FT peaks would not correspond to the magnitude of the actual membrane waves that originated them, thus providing a less intuitive readout.

The FT curve allowed us to identify and quantify the most prominent spatial frequencies and obtain relevant information about the dynamics of NE fluctuation. For the cell in prophase exemplified in Fig. 3D-G, the highest FT peak, with a wavelength of 25 μm (half of the nucleus perimeter), was the result of the large membrane displacement seen around the 15 and 40 μm arc landmarks in Fig. 3E,F. As prophase progressed, exertion of compression forces in these two separate points made the nuclear membrane wobble, with a wavelength that was half of the membrane perimeter (Fig. S4A). In addition, the FT analysis allowed the identification of membrane 'wrinkles' with spatial signatures defined by wavelengths of approximately 10, 5 and 4 μm (Fig. 3F,G). Trackosome captures these spatial signatures with high accuracy, even for curvatures with amplitudes at the subpixel level under noisy backgrounds (Fig. S4B-I).

To help uncover the processes behind these observed spatial frequencies, membrane fluctuations were calculated for cells in early mitosis and interphase (Fig. 4A,B). We calculated the majorant u_f for all cells (as in Fig. 3G) and then the median curve across trials for each group. Our results showed a significant difference in the FT curves of the two groups (Fig. 4B). In interphase, the magnitude of the fluctuations was very low through the entire spectrum of wavelengths, indicating that the membrane barely deviated from its basal position. Still, the u_f magnitude was above the noise floor established by the formaldehyde curve. This behavior changed in prophase, as there was an increase in the fluctuation amplitude for the entire range of wavelengths. This increase was particularly significant for the low frequency components, reflecting the occurrence of nucleus-wide deformations as described above.

Journal of Cell Science (2020) 133, jcs252254. doi:10.1242/jcs.252254

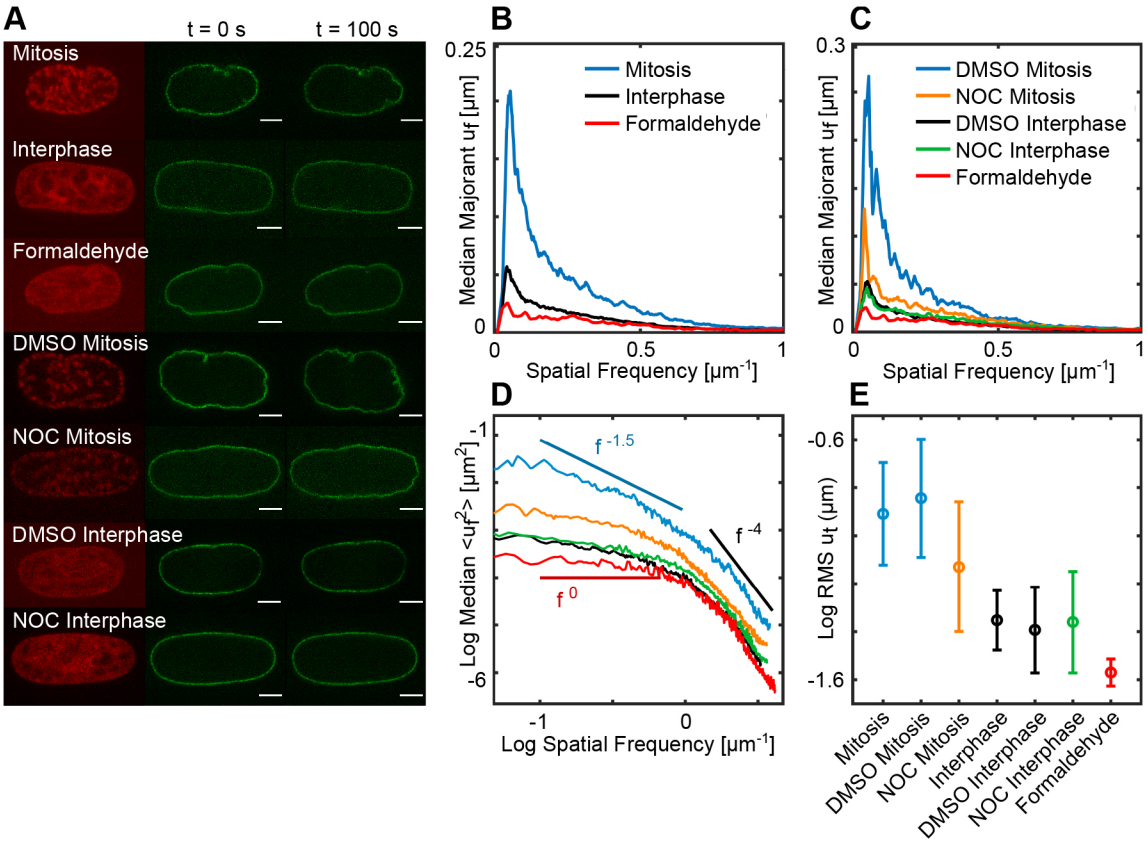

Fig. 4. Nuclear membrane fluctuations vary with the stage of the cell cycle and the physiological treatment. (A) Representative images of H2B-mCherry for each experimental group. The phase of the cell cycle is evidenced by the marked histone (red), taken from the first frame of each video. The nuclear envelope (green) is shown at two different time stamps to illustrate the degree of membrane undulation in each group. (B) Median of the majorant frequency-dependent fluctuations, u_f, obtained for groups of cells in interphase (n=44) and early mitosis (n=26). The curve for cells fixed with formaldehyde (n=4) was also included to set the noise limit. (C) Median of the majorant u_f obtained for groups of cells in interphase and mitosis, treated with DMSO (n=25 and n=15, respectively), nocodazole (NOC) (n=17 and n=16, respectively) and fixed with formaldehyde (n=4). NOC caused a significant decrease in the membrane fluctuations in mitosis. (D) Median across cells of the average FT of the squared fluctuations of each cell, $\langle u_f^2 \rangle$, for the groups represented in C. In logarithmic scales, the $\langle u_f^2 \rangle$ curves show regions dominated by different frequency dependencies, limited by the solid lines with slopes f^0, $f^{-1.5}$ and f^{-4}. (E) Mean and standard deviation of the log root mean square (RMS) of the fluctuations for all the tested groups. Using a logarithmic scale, the RMS fluctuations distributions are approximately normal and can thus be described by their mean value and standard deviation. Scale bars: 5 µm.

Fluctuations of the NE are known to depend on the cytoskeleton and, in particular, on the microtubule (MT) network (Chu et al., 2017; Hampoelz et al., 2011). To assess whether Trackosome was sensitive enough to detect these changes, we treated cells with low doses of nocodazole (NOC) to suppress the polymerization of MTs without affecting overall cell structure. Interphase cells treated with NOC had an FT curve similar to the control curve obtained for interphase cells treated with DMSO only (Fig. 4A,C). On the other hand, nuclear fluctuations of mitotic cells were significantly altered with the addition of NOC. The FT obtained for this experimental condition showed a decrease in the low-frequency peak compared with the control group. This suggests that disruption of the MT cytoskeleton led to a decreased nuclear compression, which is in agreement with reports that the MTs induce large-scale deformations of the NE (Hampoelz et al., 2011; Schreiner et al., 2015). The frequency components beyond the peak were also severely attenuated, which means that the shorter membrane wrinkles were also mitigated. Most of these effects can be qualitatively evaluated by examining the nuclei images directly (Fig. 4A), but Trackosome provides a precise quantification.

Biological membranes exhibit passive fluctuations, which are thermally excited at physiological temperatures. The equilibrium properties of these undulating systems can be modeled by Helfrich-type models (Helfrich, 1978). To evaluate the spectral dependencies in line with Helfrich theory, we calculated the average FT of the squared fluctuations for each cell, $\langle u_f^2 \rangle$, and then the median curve across cells for each group. The curves of the fluctuations obtained for the NOC and control groups showed regions with distinct spectral dependencies (Fig. 4D). For frequencies above 1.5 µm^{-1} (wavelengths below 0.7 µm), the FT curves followed a f^{-4} power law, consistent with what is expected for thermally driven fluctuations at short wavelengths (Brandt et al., 2011). At lower frequencies, each group followed a different power law, ranging from close to f^0 for formaldehyde, up to $f^{-1.5}$ for the control group in mitosis. These can be attributed to different nonequilibrium active forces governing each system. It is important to note that in Helfrich theory these spectral dependencies are defined in terms of the adimensional wavenumber q, and not spatial frequency. However, for the frequency ranges marked by the solid lines in Fig. 4D, the slopes were equivalent in both scales (Fig. S4J-L).

Finally, we compared the fluctuation amplitude [in terms of log root mean square (RMS) of u_t as in Fig. 3C, right] for all groups (Fig. 4E). NOC led to a significant decrease in the fluctuation amplitude during prophase. Importantly, this decrease was not caused by DMSO, because prophase cells in the presence of DMSO exhibited higher fluctuations than the untreated prophase cells. Also,

Journal of Cell Science (2020) 133, jcs252254. doi:10.1242/jcs.252254

the fluctuations obtained for the interphase cells were similar among the different groups and the range of amplitudes was consistent with those already described in the literature (Schreiner et al., 2015).

Overall, our results indicate that nuclear membrane fluctuations increase as cells transition from interphase to mitosis and that interfering with the MT network significantly reduces the large scale deformations of the nucleus during this stage.

DISCUSSION

Recent developments in light microscopy have generated extensive datasets that allow unprecedented access to subcellular events with high spatiotemporal resolution. Here, we report on Trackosome, a new open-source software that enables an automated quantitative analysis of the spatiotemporal dynamics of subcellular structures even in conditions of low signal-to-noise ratio. During the transition from G2 to mitosis, chromosomes condense (Antonin and Neumann, 2016), cells round up (Matthews et al., 2012) and centrosomes separate (Whitehead et al., 1996). In this context, the extent of centrosome separation at the time of NEB remains a matter of debate. Although some reports show that cells can enter mitosis with unseparated centrosomes (Kaseda et al., 2012; Whitehead et al., 1996), others indicate that centrosomes are fully separated at NEB (Magidson et al., 2011; Mardin et al., 2013; Nunes et al., 2020). These discrepancies highlight the need to determine carefully how the events leading up to mitosis are coordinated to ensure efficient spindle assembly. By using the different modules available on Trackosome, we were able to correlate centrosome movement accurately and centrosome-nucleus axis reorientation during mitotic entry. Our results, using cells seeded on fibronectin micropatterns, indicate that centrosomes are fully separated before NEB and that their movement is coordinated to optimize their positioning on opposite sides of the nucleus (Magidson et al., 2011), in contrast to previous observations (Waters et al., 1993). This coordination was evidenced using elliptical coordinates to describe the centrosome trajectories around the nucleus. Interestingly, the high correlation scores between movement components of both centrosomes strongly indicate a mechanical coupling between the two structures. This coupling could be provided by specific pools of dynein on the cell cortex (Kotak et al., 2012; Woodard et al., 2010) or at the NE (Bolhy et al., 2011; Splinter et al., 2012), which are known to generate pulling forces on centrosomal microtubules to position asters (Laan et al., 2012). Determining the exact nature of this mechanical coupling between the centrosomes during mitotic entry will be of interest in the future.

The mechanical properties of the nucleus depend on the chromatin condensation state (Stephens et al., 2017, 2018) and the nuclear lamina (Lammerding et al., 2006). Given that Lamin A levels (Chu et al., 2017; Moir et al., 2000) and chromatin compaction (Hinde et al., 2012) change throughout the cell cycle, it is possible that the mechanical properties of the nucleus change accordingly. In agreement, NE fluctuations, which reflect forces imposed on the nucleus, were shown to vary depending on the cell cycle stage (Chu et al., 2017). However, whether the mechanical properties of the nucleus change during the transition from G2 to mitosis, when mitotic chromosomes condense and the nuclear lamina disassembles, remains unclear. Here, we report on a new tool for analyzing NE fluctuations during mitotic entry that measures orthogonal displacements relative to the medial position of the nuclear membrane. We reveal that chromosome condensation, together with microtubules, triggers significant changes in the spatial pattern of NE fluctuations as cells prepare to enter mitosis. To the best of our knowledge, it is the first time that the transition from G2 to prophase has been characterized in terms of NE fluctuations. In the future, it will be interesting to determine how these fluctuations reflect the mechanical properties of the nucleus.

The novel algorithms compiled in the computational toolbox Trackosome provide a reliable and accurate instrument with subpixel precision to help uncover new elements in the spatiotemporal dynamics of subcellular structures. Importantly, Trackosome is not restricted to centrosomes and the nucleus or cell membrane; its algorithms can be used to track other subcellular structures, providing these structures can be adequately segmented from 3D live imaging data (in its current version, Trackosome can simultaneously track two particles and two membranes sets). Moreover, this toolbox has the potential to be adapted to other experimental conditions such as the study of cell migration and cell polarity, where the capacity to analyze dynamic datasets with high accuracy is highly relevant. Being specifically developed in MATLAB and made publically available as open-source software allows other researchers to easily modify Trackosome and integrate additional functions or metrics to suit their needs.

MATERIALS AND METHODS

Biological methods

Cell culture

Cell lines were cultured in Dulbecco's modified Eagle medium (DMEM; Life Technologies) supplemented with 10% fetal bovine serum (FBS; Life Technologies) and grown in a 37°C humidified incubator with 5% CO_2. The HeLa POM121-3×GFP/H2B-mCherry cell line was a kind gift from the laboratory of Katharine Ullman (University of Utah, Salt Lake City, UT, USA). The HeLa cell line expressing histone H2B-GFP/mRFP-α-tubulin was generated in our laboratory using lentiviral vectors. All cell lines were authenticated in the laboratory of origin. All cell lines used in this study are routinely tested for mycoplasma contamination and always found to be negative.

Micropatterning

Micropatterns to control individual cell shape and adhesion pattern were produced as previously described (Azioune et al., 2009). Briefly, glass coverslips (22×22 mm No. 1.5; VWR) were activated with plasma (Zepto Plasma System, Diener Electronic) for 1 min and incubated with 0.1 mg/ml of PLL(20)-g[3,5]-PEG(2) (SuSoS) in 10 mM HEPES at pH 7.4, for 1 h at room temperature. After rinsing and air-drying, the coverslips were placed on a synthetic quartz photomask (Delta Mask), previously activated with deep-UV light (PSD-UV, Novascan Technologies) for 5 min. MiliQ water (3 µl) was used to seal each coverslip to the mask. The coverslips were then irradiated through the photomask with the UV lamp for 5 min. Afterwards, coverslips were incubated with 25 µg/ml of fibronectin (Sigma-Aldrich) and 5 µg/ml of Alexa Fluor 546 or 647-conjugated fibrinogen (ThermoFisher Scientific) in 100 mM $NaHCO_3$ at pH 8.6, for 1 h at room temperature. Cells were seeded at a density of 50,000 cells/coverslip and allowed to spread for 10-15 h before imaging. Non-attached cells were removed by changing the medium 2-5 h after seeding.

Time-lapse microscopy

For time-lapse microscopy, 12-24 h before the experiments, 5×10^4 cells were seeded on coverslips coated with FBN (25 µg/ml; F1141, Sigma). Prior to each experiment, cell culture medium was changed from DMEM with 10% FBS to Leibovitz-L15 medium (Life Technologies) supplemented with 10% FBS and Antibiotic-Antimycotic 100× (AAS; Life Technologies). When SiR dyes were used, they were added to the culture medium 30-60 min before acquisition (20 nM SiR-tubulin or 10 nM SiR-DNA; Spirochrome). Where stated, nocodazole was added to the cells 30 min before the experiment (20 nM; Sigma-Aldrich). Live-cell imaging was performed using temperature-controlled Nikon TE2000 microscopes equipped with a modified Yokogawa CSU-X1 spinning-disc head (Yokogawa Electric), an electron multiplying iXon+ DU-897 EM-CCD

camera (Andor) and a filter-wheel. Three laser lines were used for excitation at 488, 561 and 647 nm. For nuclear membrane fluctuations, an oil-immersion 100×1.4 NA Plan-Apo DIC (Nikon) was used. All the remaining experiments were done with an oil-immersion 60×1.4 NA Plan-Apo DIC (Nikon). Image acquisition was controlled by NIS Elements AR software. For centrosome tracking, 17-21 z-stacks with a 0.5 µm separation were collected every 20 s or, to analyze centrosome correlations, every 10 s. For NE fluctuation measurements, a single z-stack was collected every 100 ms.

Trackosome toolbox: Centrosome Dynamics

Trackosome is made publically available (open-source) as a platform-independent MATLAB toolbox and can be downloaded from https://github.com/Trackosome.

Tracking algorithm

A 3D Laplacian of Gaussian filter is applied to the video of centrosomes to highlight centrosome-like blobs. The user must then select the approximate position of the two centrosomes in an XY maximum projection of the first frame. These are the seeding points for the tracking loop that follows. For each frame, two 3D regions of interest (ROIs) are centered at the coordinates of the centrosomes obtained for the previous frame (for the first frame, it uses the coordinates selected by the user). The ROIs are large enough to encompass the centrosome displacements between frames. This ensures that the ROIs, centered in the coordinates of the centrosomes at the previous frame, still contain the centrosomes in the current frame. The ROIs are thresholded to isolate regions of high intensity. Then, each ROI is iteratively shortened, one-dimension at a time, until it confines a high-intensity blob with the approximate size of the centrosome. Once each centrosome is enclosed by a 3D mask, the centroids are found by projecting the masked intensities along the three axes and fitting a Gaussian curve to each intensity profile – the coordinates of the centrosome correspond to the peaks of the fitted Gaussian curves (Fig. S3E).

Nuclear and cellular membrane reconstruction

The images from each video (nucleus and cellular membrane) are filtered with a 4D (three spatial dimensions and one temporal dimension) average filter. Then, they are binarized using Otsu's method and submitted to an iterative set of morphological operations intended to create a closed, smooth, binary volume. The membrane of each structure corresponds to the outer pixels of their binary volume. The major axes of the cell and nucleus are obtained by calculating the principal components of the binary volumes for each frame.

Correlation of centrosome trajectories

The correlations among displacements of the centrosomes were evidenced by defining their movements as two ellipsoidal trajectories surrounding the approximately ellipsoidal nucleus (Fig. S3F-H). The nucleus was centered to ensure a common centroid in each frame. The median nucleus was obtained by calculating the median binary volume across time. The videos were analyzed until NE breakdown. An ellipsoid was fitted to the median nucleus, setting the coordinate system used to define the ellipsoidal trajectories. The trajectories of the centrosomes were normalized with regards to the centroid of the nucleus for each frame. The transformed trajectories were converted to ellipsoidal coordinates, using the fitted ellipsoid as a referential of the coordinate system. The trajectories were also characterized by the norm of the ellipsoidal velocity and acceleration, and by their decomposition along the latitude, longitude and altitude directions at each point. Once all the features of both centrosome trajectories were calculated, the correlation matrix was directly obtained. We only included videos with long and changing centrosome trajectories, because short monotonic trajectories would invariantly have high, but misleading, correlation coefficients. We also excluded videos with a nonstationary nucleus because a moving referential would lead to fallacious correlation values.

Trackosome toolbox: Membrane Fluctuations

We consider that the points of the model-free membrane move in a direction perpendicular to its surface. This is an important novelty, compared with the frequently used methodology that relies on the, much easier to calculate, but flawed, radial direction (see Fig. 3A). We define the fluctuations as being the distance from each point of the median membrane to the membrane at a given frame, along a direction normal to the median membrane. The membranes are segmented for all frames and then centered, assuring a common centroid among frames. To calculate the basal position (the reference membrane) of the NE, we calculate the median projection of the centered frames and segment the resulting membrane. Each point of the reference membrane is associated with a normal vector that defines the direction of the membrane displacements. The fluctuations are then measured by calculating the distance from the reference membrane to the membrane of each frame, along the directions defined by the normal vectors (see Fig. S3I,J).

Acknowledgements

The authors would like to thank Margarida Dantas for the critical reading of the manuscript and Helder Maiato for providing access to microscopes and equipment. The authors would like to thank Katharine Ullman for the HeLa POM121-3×GFP/H2B-mCherry.

Competing interests

The authors declare no competing or financial interests.

Author contributions

Conceptualization: D.C., J.G.F., P.A.; Methodology: D.C., J.G.F., P.A.; Software: D.C., P.A.; Formal analysis: D.C., J.G.F., P.A.; Investigation: D.C., V.N., J.T.L., J.G.F., P.A.; Resources: J.G.F., P.A.; Data curation: D.C., V.N., J.T.L., J.G.F., P.A.; Writing - original draft: D.C., J.G.F., P.A.; Writing - review & editing: D.C., J.G.F., P.A.; Supervision: J.G.F., P.A.; Project administration: P.A.; Funding acquisition: J.G.F., P.A.

Funding

This work was funded by grants from Fundo Europeu de Desenvolvimento Regional (FEDER) through the COMPETE 2020 - Operacional Programme for Competitiveness and Internationalization (POCI), Portugal 2020, and by Portuguese funds through Fundação para a Ciência e a Tecnologia/Ministério da Ciência, Tecnologia e Ensino Superior (FCT) in the framework of the project PTDC/BEX-BCM/1758/2014 (POCI-01–0145-FEDER-016589). V.N. is supported by grant PD/BD/135545/2018 from the BiotechHealth Fundação para a Ciência e a Tecnologia/Ministério da Ciência, Tecnologia e Ensino Superior PhD program. J.T.L. is supported by grant SFRH/BD/147169/2019 from Fundação para a Ciência e a Tecnologia/Ministério da Ciência, Tecnologia e Ensino Superior. The laboratory of Helder Maiato has received funding for research and equipment from the European Research Council (ERC) under the European Union's Horizon 2020 research and innovation program (grant agreement No 681443).

Supplementary information

Supplementary information available online at
https://jcs.biologists.org/lookup/doi/10.1242/jcs.252254.supplemental

Peer review history

The peer review history is available online at
https://jcs.biologists.org/lookup/doi/10.1242/jcs.252254.reviewer-comments.pdf

References

Almonacid, M., Al Jord, A., El-Hayek, S., Othmani, A., Coulpier, F., Lemoine, S., Miyamoto, K., Grosse, R., Klein, C., Piolot, T. et al. (2019). Active fluctuations of the nuclear envelope shape the transcriptional dynamics in oocytes. *Dev. Cell* **51**, 145-157.e10. doi:10.1016/j.devcel.2019.09.010

Antonin, W. and Neumann, H. (2016). Chromosome condensation and decondensation during mitosis. *Curr. Opin. Cell Biol.* **40**, 15-22. doi:10.1016/j.ceb.2016.01.013

Azioune, A., Storch, M., Bornens, M., Théry, M. and Piel, M. (2009). Simple and rapid process for single cell micro-patterning. *Lab. Chip* **9**, 1640. doi:10.1039/b821581m

Blanchoud, S., Budirahardja, Y., Naef, F. and Gönczy, P. (2010). ASSET: a robust algorithm for the automated segmentation and standardization of early Caenorhabditis elegans embryos. *Dev. Dyn.* **239**, 3285-3296. doi:10.1002/dvdy.22486

Bolhy, S., Bouhlel, I., Dultz, E., Nayak, T., Zuccolo, M., Gatti, X., Vallee, R., Ellenberg, J. and Doye, V. (2011). A Nup133-dependent NPC-anchored network tethers centrosomes to the nuclear envelope in prophase. *J. Cell Biol.* **192**, 855-871. doi:10.1083/jcb.201007118

Boudreau, V., Chen, R., Edwards, A., Sulaimain, M. and Maddox, P. S. (2019). PP2A-B55/SUR-6 collaborates with the nuclear lamina for centrosome separation during mitotic entry. *Mol. Biol. Cell* **30**, 876-886. doi:10.1091/mbc.E18-10-0631

Brandt, E. G., Braun, A. R., Sachs, J. N., Nagle, J. F. and Edholm, O. (2011). Interpretation of fluctuation spectra in lipid bilayer simulations. *Biophys. J.* **100**, 2104-2111. doi:10.1016/j.bpj.2011.03.010

Cao, J., Crest, J., Fasulo, B. and Sullivan, W. (2010). Cortical actin dynamics facilitate early-stage centrosome separation. *Curr. Biol.* **20**, 770-776. doi:10.1016/j.cub.2010.02.060

Caragine, C. M., Haley, S. C. and Zidovska, A. (2018). Surface fluctuations and coalescence of nucleolar droplets in the human cell nucleus. *Phys. Rev. Lett.* **121**, 148101. doi:10.1103/PhysRevLett.121.148101

Champion, L., Linder, M. I. and Kutay, U. (2017). Cellular reorganization during mitotic entry. *Trends Cell Biol.* **27**, 26-41. doi:10.1016/j.tcb.2016.07.004

Chu, F.-Y., Haley, S. C. and Zidovska, A. (2017). On the origin of shape fluctuations of the cell nucleus. *Proc. Natl. Acad. Sci. USA* **114**, 10338-10343. doi:10.1073/pnas.1702226114

Collins, E., Mann, B. J. and Wadsworth, P. (2014). Eg5 restricts anaphase B spindle elongation in mammalian cells. *Cytoskeleton* **71**, 136-144. doi:10.1002/cm.21158

Dao, V. T., Dupuy, A. G., Gavet, O., Caron, E. and de Gunzburg, J. (2009). Dynamic changes in Rap1 activity are required for cell retraction and spreading during mitosis. *J. Cell Sci.* **122**, 2996-3004. doi:10.1242/jcs.041301

De Simone, A., Nédélec, F. and Gönczy, P. (2016). Dynein transmits polarized actomyosin cortical flows to promote centrosome separation. *Cell Rep.* **14**, 2250-2262. doi:10.1016/j.celrep.2016.01.077

Eliceiri, K. W., Berthold, M. R., Goldberg, I. G., Ibáñez, L., Manjunath, B. S., Martone, M. E., Murphy, R. F., Peng, H., Plant, A. L., Roysam, B. et al. (2012). Biological imaging software tools. *Nat. Methods* **9**, 697-710. doi:10.1038/nmeth.2084

Georgatos, S. D., Pyrpasopoulou, A. and Theodoropoulos, P. A. (1997). Nuclear envelope breakdown in mammalian cells involves stepwise lamina disassembly and microtubule-drive deformation of the nuclear membrane. *J. Cell Sci.* **110**, 2129-2140.

Gerlich, D., Beaudouin, J., Gebhard, M., Ellenberg, J. and Eils, R. (2001). Four-dimensional imaging and quantitative reconstruction to analyse complex spatiotemporal processes in live cells. *Nat. Cell Biol.* **3**, 852-855. doi:10.1038/ncb0901-852

Hampoelz, B., Azou-Gros, Y., Fabre, R., Markova, O., Puech, P.-H. and Lecuit, T. (2011). Microtubule-induced nuclear envelope fluctuations control chromatin dynamics in Drosophila embryos. *Development* **138**, 3377-3386. doi:10.1242/dev.065706

Helfrich, W. (1978). Steric interaction of fluid membranes in multilayer systems. *Zeitschrift für Naturforschung A* **33**, 305-315. doi:10.1515/zna-1978-0308

Hinde, E., Cardarelli, F., Digman, M. A. and Gratton, E. (2012). Changes in chromatin compaction during the cell cycle revealed by micrometer-scale measurement of molecular flow in the nucleus. *Biophys. J.* **102**, 691-697. doi:10.1016/j.bpj.2011.11.4026

Jahed, Z. and Mofrad, M. R. K. (2019). The nucleus feels the force, LINCed in or not!. *Curr. Opin. Cell Biol.* **58**, 114-119. doi:10.1016/j.ceb.2019.02.012

Kaseda, K., McAinsh, A. D. and Cross, R. A. (2012). Dual pathway spindle assembly increases both the speed and the fidelity of mitosis. *Biol. Open* **1**, 12-18. doi:10.1242/bio.2011012

Kotak, S., Busso, C. and Gönczy, P. (2012). Cortical dynein is critical for proper spindle positioning in human cells. *J. Cell Biol.* **199**, 97-110. doi:10.1083/jcb.201203166

Laan, L., Pavin, N., Husson, J., Romet-Lemonne, G., van Duijn, M., López, M. P., Vale, R. D., Jülicher, F., Reck-Peterson, S. L., Dogterom, M. et al. (2012). Cortical dynein controls microtubule dynamics to generate pulling forces that position microtubule asters. *Cell* **148**, 502-514. doi:10.1016/j.cell.2012.01.007

Lammerding, J., Fong, L. G., Ji, J. Y., Reue, K., Stewart, C. L., Young, S. G. and Lee, R. T. (2006). Lamins A and C but not lamin B1 regulate nuclear mechanics. *J. Biol. Chem.* **281**, 25768-25780. doi:10.1074/jbc.M513511200

Magidson, V., O'Connell, C. B., Lončarek, J., Paul, R., Mogilner, A. and Khodjakov, A. (2011). The spatial arrangement of chromosomes during prometaphase facilitates spindle assembly. *Cell* **146**, 555-567. doi:10.1016/j.cell.2011.07.012

Mahen, R. (2018). Stable centrosomal roots disentangle to allow interphase centriole independence. *PLoS Biol.* **16**, e2003998. doi:10.1371/journal.pbio.2003998

Mardin, B. R., Isokane, M., Cosenza, M. R., Krämer, A., Ellenberg, J., Fry, A. M. and Schiebel, E. (2013). EGF-induced centrosome separation promotes mitotic progression and cell survival. *Dev. Cell* **25**, 229-240. doi:10.1016/j.devcel.2013.03.012

Matthews, H. K., Delabre, U., Rohn, J. L., Guck, J., Kunda, P. and Baum, B. (2012). Changes in Ect2 localization couple actomyosin-dependent cell shape changes to mitotic progression. *Dev. Cell* **23**, 371-383. doi:10.1016/j.devcel.2012.06.003

Mchedlishvili, N., Matthews, H. K., Corrigan, A. and Baum, B. (2018). Two-step interphase microtubule disassembly aids spindle morphogenesis. *BMC Biol.* **16**, 14. doi:10.1186/s12915-017-0478-z

Moir, R. D., Yoon, M., Khuon, S. and Goldman, R. D. (2000). Nuclear lamins A and B1: different pathways of assembly during nuclear envelope formation in living cells. *J. Cell Biol.* **151**, 1155-1168. doi:10.1083/jcb.151.6.1155

Nunes, V., Dantas, M., Castro, D., Vitiello, E., Wang, I., Carpi, N., Balland, M., Piel, M., Aguiar, P., Maiato, H. et al. (2020). Centrosome-nuclear axis repositioning drives the assembly of a bipolar spindle scaffold to ensure mitotic fidelity. *Mol. Biol. Cell* **31**, 1675-1690. doi:10.1091/mbc.E20-01-0047

Otsuka, S., Steyer, A. M., Schorb, M., Hériché, J.-K., Hossain, M. J., Sethi, S., Kueblbeck, M., Schwab, Y., Beck, M., Ellenberg, J. et al. (2018). Postmitotic nuclear pore assembly proceeds by radial dilation of small membrane openings. *Nat. Struct. Mol. Biol.* **25**, 21-28. doi:10.1038/s41594-017-0001-9

Raaijmakers, J. A., van Heesbeen, R. G. H. P., Meaders, J. L., Geers, E. F., Fernandez-Garcia, B., Medema, R. H. and Tanenbaum, M. E. (2012). Nuclear envelope-associated dynein drives prophase centrosome separation and enables Eg5-independent bipolar spindle formation. *EMBO J.* **31**, 4179-4190. doi:10.1038/emboj.2012.272

Rosenblatt, J., Cramer, L. P., Baum, B. and McGee, K. M. (2004). Myosin II-dependent cortical movement is required for centrosome separation and positioning during mitotic spindle assembly. *Cell* **117**, 361-372. doi:10.1016/S0092-8674(04)00341-1

Schreiner, S. M., Koo, P. K., Zhao, Y., Mochrie, S. G. J. and King, M. C. (2015). The tethering of chromatin to the nuclear envelope supports nuclear mechanics. *Nat. Commun.* **6**, 7159. doi:10.1038/ncomms8159

Splinter, D., Razafsky, D. S., Schlager, M. A., Serra-Marques, A., Grigoriev, I., Demmers, J., Keijzer, N., Jiang, K., Poser, I., Hyman, A. A. et al. (2012). BICD2, dynactin, and LIS1 cooperate in regulating dynein recruitment to cellular structures. *Mol. Biol. Cell* **23**, 4226-4241. doi:10.1091/mbc.e12-03-0210

Stephens, A. D., Banigan, E. J., Adam, S. A., Goldman, R. D. and Marko, J. F. (2017). Chromatin and lamin A determine two different mechanical response regimes of the cell nucleus. *Mol. Biol. Cell* **28**, 1984-1996. doi:10.1091/mbc.e16-09-0653

Stephens, A. D., Liu, P. Z., Banigan, E. J., Almassalha, L. M., Backman, V., Adam, S. A., Goldman, R. D. and Marko, J. F. (2018). Chromatin histone modifications and rigidity affect nuclear morphology independent of lamins. *Mol. Biol. Cell* **29**, 220-233. doi:10.1091/mbc.E17-06-0410

Stephens, A. D., Banigan, E. J. and Marko, J. F. (2019). Chromatins physical properties shape the nucleus and its functions. *Curr. Opin. Cell Biol.* **58**, 76-84. doi:10.1016/j.ceb.2019.02.006

Stiff, T., Echegaray-Iturra, F. R., Pink, H. J., Herbert, A., Reyes-Aldasoro, C. C. and Hochegger, H. (2020). Prophase-specific perinuclear actin coordinates centrosome separation and positioning to ensure accurate chromosome segregation. *Cell Rep.* **31**, 107681. doi:10.1016/j.celrep.2020.107681

Tanenbaum, M. E. and Medema, R. H. (2010). Mechanisms of centrosome separation and bipolar spindle assembly. *Dev. Cell* **19**, 797-806. doi:10.1016/j.devcel.2010.11.011

Tinevez, J.-Y., Perry, N., Schindelin, J., Hoopes, G. M., Reynolds, G. D., Laplantine, E., Bednarek, S. Y., Shorte, S. L. and Eliceiri, K. W. (2017). TrackMate: an open and extensible platform for single-particle tracking. *Methods* **115**, 80-90. doi:10.1016/j.ymeth.2016.09.016

Versaevel, M., Grevesse, T. and Gabriele, S. (2012). Spatial coordination between cell and nuclear shape within micropatterned endothelial cells. *Nat. Commun.* **3**, 671. doi:10.1038/ncomms1668

Waters, J. C., Cole, R. W. and Rieder, C. L. (1993). The force-producing mechanism for centrosome separation during spindle formation in vertebrates is intrinsic to each aster. *J. Cell Biol.* **122**, 361-372. doi:10.1083/jcb.122.2.361

Whitehead, C. M., Winkfein, R. J. and Rattner, J. B. (1996). The relationship of HsEg5 and the actin cytoskeleton to centrosome separation. *Cell Motil. Cytoskelet.* **35**, 298-308. doi:10.1002/(SICI)1097-0169(1996)35:4<298::AID-CM3>3.0.CO;2-3

Woodard, G. E., Huang, N.-N., Cho, H., Miki, T., Tall, G. G. and Kehrl, J. H. (2010). Ric-8A and Giα recruit LGN, NuMA, and dynein to the cell cortex to help orient the mitotic spindle. *Mol. Cell. Biol.* **30**, 3519-3530. doi:10.1128/MCB.00394-10

Yamashita, N., Morita, M., Legant, W. R., Chen, B.-C., Betzig, E., Yokota, H. and Mimori-Kiyosue, Y. (2015). Three-dimensional tracking of plus-tips by lattice light-sheet microscopy permits the quantification of microtubule growth trajectories within the mitotic apparatus. *J. Biomed. Opt.* **20**, 101206. doi:10.1117/1.JBO.20.10.101206

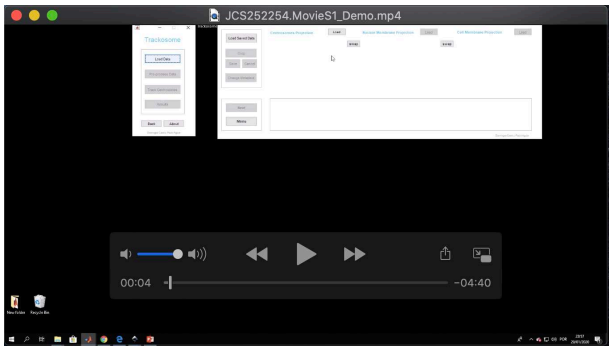

Movie 1. Demonstration of Centrosome Dynamics module of Trackosome. Demonstration of how to: load 3D live-imaging data from centrosomes, nuclear membrane and cellular membrane; perform centrosome tracking and correct tracking mistakes; explore and save the results; reload previously saved data.

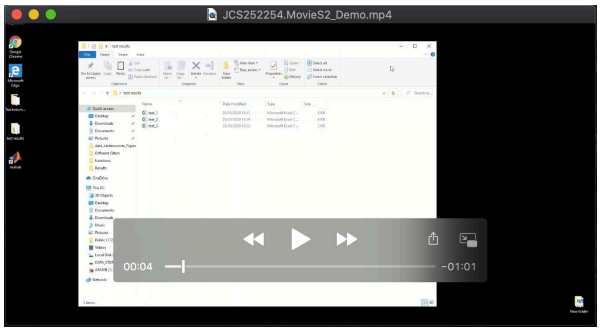

Movie 2. Demonstration of results compilation in Centrosome Dynamics module of Trackosome. Demonstration of how to compile the results from different files analyzed with the Centrosome Dynamics module into a single excel file.

Movie 3. Demonstration of the membrane corrections in Centrosome Dynamics module. Demonstration of how to correct errors in the segmentation of the nuclear membrane and cellular membrane in Centrosome Dynamics module.

Journal of Cell Science • Supplementary information

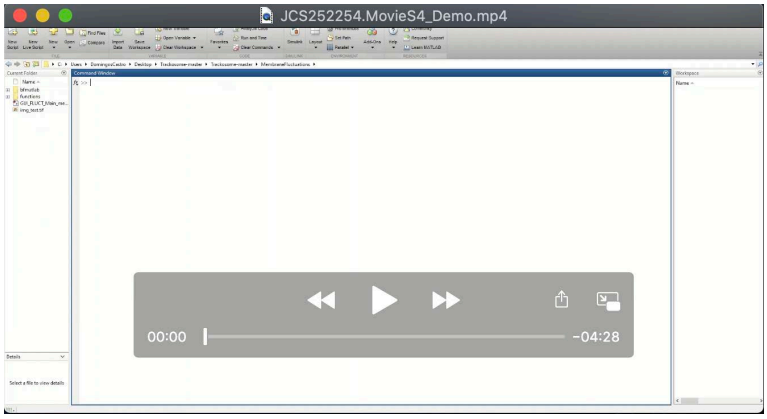

Movie 4. Demonstration of Nuclear Envelope Fluctuations module of Trackosome. Demonstration of how to: load files from 2D live-imaging data of the nuclear envelope; segment the nuclear envelope and correct segmentation mistakes; analyze, correct and save fluctuation results; reload previously saved data.

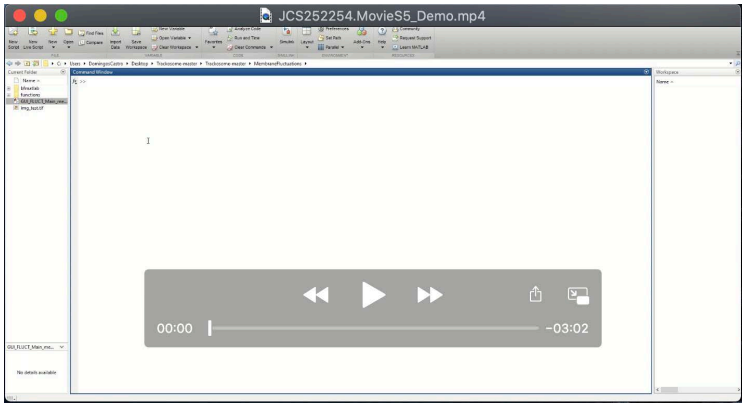

Movie 5. Demonstration of batch mode analysis in Nuclear Envelope Fluctuations module of Trackosome. Demonstration of how to: load multiple 2D live-imaging data files of the nuclear envelope; correct membrane segmentations and fluctuation results for each individual file; save the files of interest.

Journal of Cell Science • Supplementary information

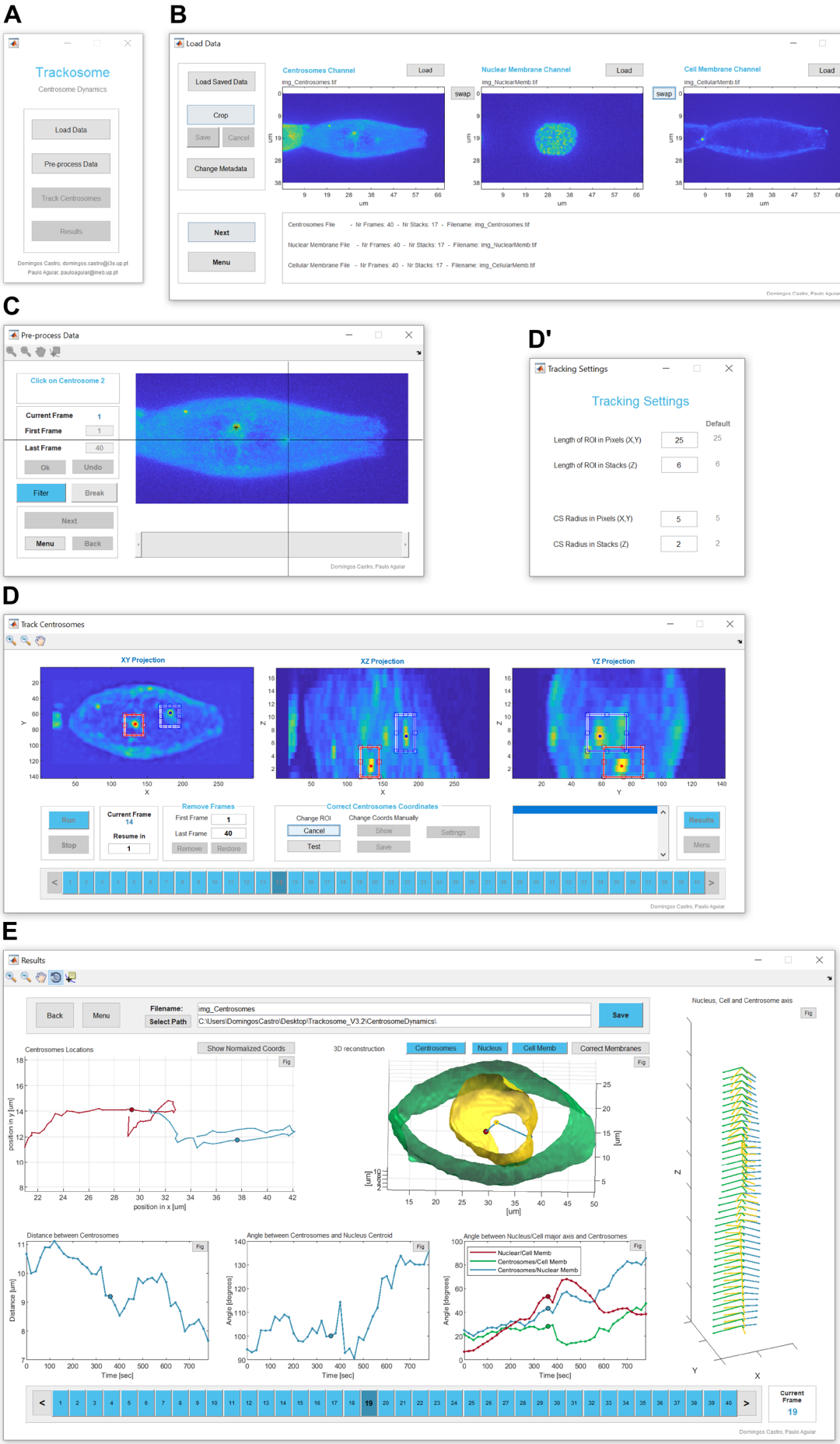

Journal of Cell Science • Supplementary information

Figure S1. Trackosome User Interface: Centrosome Dynamics module. (A**)** Main menu to open the windows shown in B, C, D and E. (B) Load data window, where the user can import the 3D live-cell imaging videos from the centrosomes, nuclear membrane and cellular membrane (.tiff, .mat, .nd2). It is also possible to load .mat files previously exported by Trackosome ("Load Saved Data" button). These populate the entire interface with the data contained in the file, allowing the user to reexamine previous analysis. (C) Pre-processing window to filter the centrosomes channel, trim the videos, and select the approximate initial coordinates of the centrosomes. (D) Centrosomes tracking window. The user can follow the tracking results for each frame in real-time. The algorithm can be stopped at any time to correct eventual mistakes. There are two modes of coordinates correction: 1) "Change ROI": move and resize the regions-of-interest to guarantee that they contain the centrosomes (option currently selected in the image shown); 2) "Change Coords Manually": manual selection of the new 3D coordinates of a centrosome. The algorithm can proceed from the corrected frame. These corrections can also be done after analyzing the full video. The array of blue buttons at the bottom allows the user to navigate between frames and provide visual feedback regarding the tracking status of each frame: blue - ok; yellow - problem finding the centrosomes; red - forced break due to error; gray - coordinates manually changed. The user can also discard specific frames from the analysis in the "Remove Frames" section. (D') Window to change the main settings of the tracking algorithm. (E) Results window where the user can inspect and save the results obtained. The results can be exported as .xlsx, .csv files and also a .mat file that stores all the data from the interface. The .mat file allows the user to reload the full Trackosome interface with the stored data. Also, the user can access relevant stored variables (such as the membrane reconstructions) by loading this .mat file directly on the MATLAB command window. See Movie 1.

Journal of Cell Science • Supplementary information

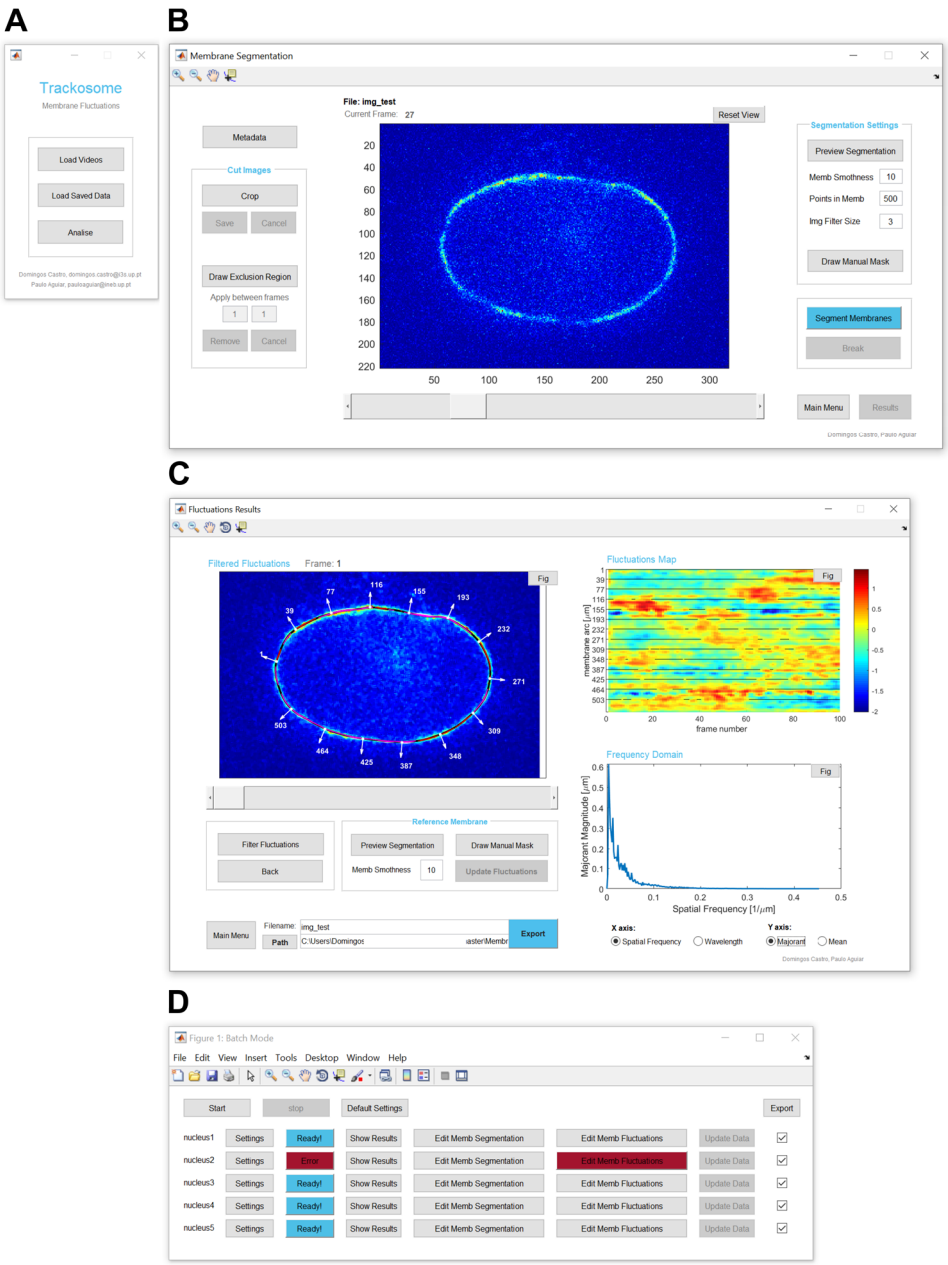

Figure S2. Trackosome User Interface: Membrane Fluctuations module. (A) Main menu to load the 2D videos (.tiff, .mat, .nd2). The loading function used is *uipickfiles* (Douglas Schwarz 2020). If only one video is selected, the user is directed to the window shown in B. If multiple files are selected, the user is directed to batch analysis mode, shown in D. It is also possible to open previously exported files and load the entire interface with the imported data. (B) Window to perform membrane segmentation. The user can edit the video before segmenting the membranes. The edit options include cropping the frames, drawing masks to guide membrane segmentation, and removing manually drawn regions from specified frames (to eliminate, for example, high intensity noise blobs located near the membrane). It is possible to preview the segmentation of any frame to optimize parameters before starting the segmentation of the entire video. (C) Results window where the user can inspect, correct and export the results obtained. The corrections include editing the reference membrane and adjusting the spatiotemporal filters

applied to the membrane fluctuations. (D) Window for batch analysis, opened if the user selects multiple videos in the Main Menu. In the window shown, five files were selected. Each file is associated with a set of buttons to edit parameters, show the results obtained, edit the membrane segmentation (opens window B), edit fluctuation results (opens window C), and activate/deactivate exporting.

Journal of Cell Science • Supplementary information

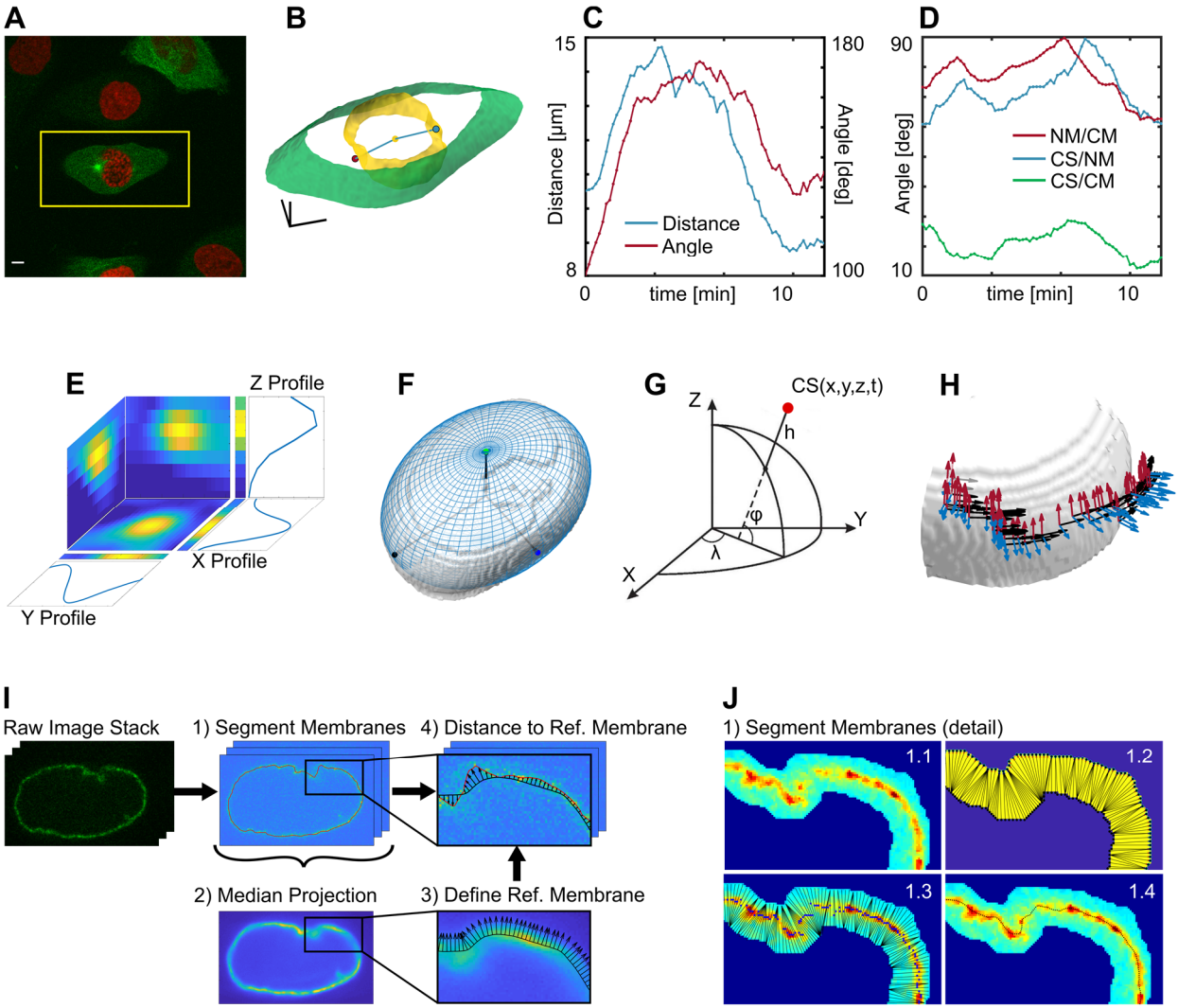

Figure S3. Details of Trackosome algorithms. (A-D) Analysis of unconstrained cells with Trackosome, to demonstrate how the algorithm can be used in multiple experimental conditions, and not only in micro-patterned cells. (A) Image of a RPE-1 cell expressing tubulin-GFP/H2B-RFP in a fibronectin coated glass coverslip. The centrosomes can be easily identified in green channel and the nucleus in the red channel. The green channel can also be used to identify the cellular membrane, because the cellular limit is clear enough for Trackosome to reconstruct it. The yellow rectangle marks the cropping performed in Trackosome to analyze a single cell - the nuclear and cellular membrane reconstruction algorithms require isolated cells. Scale-bar: 5 µm. (B) 3D reconstruction of the centrosomes, nuclear envelope and cellular membrane, for the frame shown in A. Scale-bars: 5 µm. (C) Distance (blue) and angles (red) between centrosomes. The distance between centrosomes starts decreasing once they form a 180° angle with the nucleus centroid, that is, once they are at opposite sides of the nucleus. (D) Angles formed between: centrosomes axis and the nucleus major axis (blue); centrosomes axis and the cell major axis (green); the nucleus major axis and the cell major axis (red). These curves show that the nucleus is displaced perpendicularly to the cellular membrane and the centrosomes are aligned with the cellular membrane, as shown in B. (E) Detail of the centrosome tracking algorithm (Centrosome

Dynamics module). Example of the initial region-of-interest (ROI) obtained for a centrosome at a given frame. The three planes represent the intensity sum projections of the ROI. The ROIs are centered in the coordinates of the centrosome obtained in the previous frame. The initial ROI is shortened until it confines a blob with the dimensions of the centrosome. The short ROI converges to the peaks of intensity shown in the X, Y, Z profiles. The final 3D coordinates of the centrosome are found by fitting a Gaussian curve to the intensity profiles along the X, Y and Z axes extracted from the shortened ROI. The (x,y,z) position of the centrosome corresponds to the mean value of each Gaussian curve. (F-H) Details of centrosome trajectories in ellipsoidal coordinates. (F) Ellipsoid (blue) fitted to the median nucleus (grey) used as referential for the ellipsoidal coordinates. (G) Conversion from Cartesian (x,y,z) to ellipsoidal (ϕ, λ, h) coordinates based on the referential system defined in F. The red dot represents a centrosome (CS) in a given time point (t). (H) Each point of the centrosomes trajectories is associated with an orthonormal basis defined by a latitude unit vector (red), longitude unit vector (black) and height unit vector (blue). These indicate the direction along which the ellipsoidal velocities and accelerations are calculated for each position. (I-J) Details of the membrane fluctuations algorithm (Nuclear Envelope Fluctuations module). (I) Overview of the four main steps of the algorithm: 1) membrane segmentation and centering; 2) median projection of the centered frames; 3) segmentation of the membrane obtained in 2, defining the reference membrane and the associated normal vectors; 4) Definition of the membrane fluctuations for each frame as the distance between the reference membrane and the membrane of the current frame, along the direction defined by the vectors orthogonal to the reference membrane. (J) Detail of the membrane segmentation step (1) for a given frame: 1.1) filter and mask the image; 1.2) the points that constitute the two borders of the mask are connected by the shortest segment; 1.3) find the pixel with maximum intensity for each segment defined in 1.2; 1.4) filter the positions of the pixels found in 1.3.

Journal of Cell Science • Supplementary information

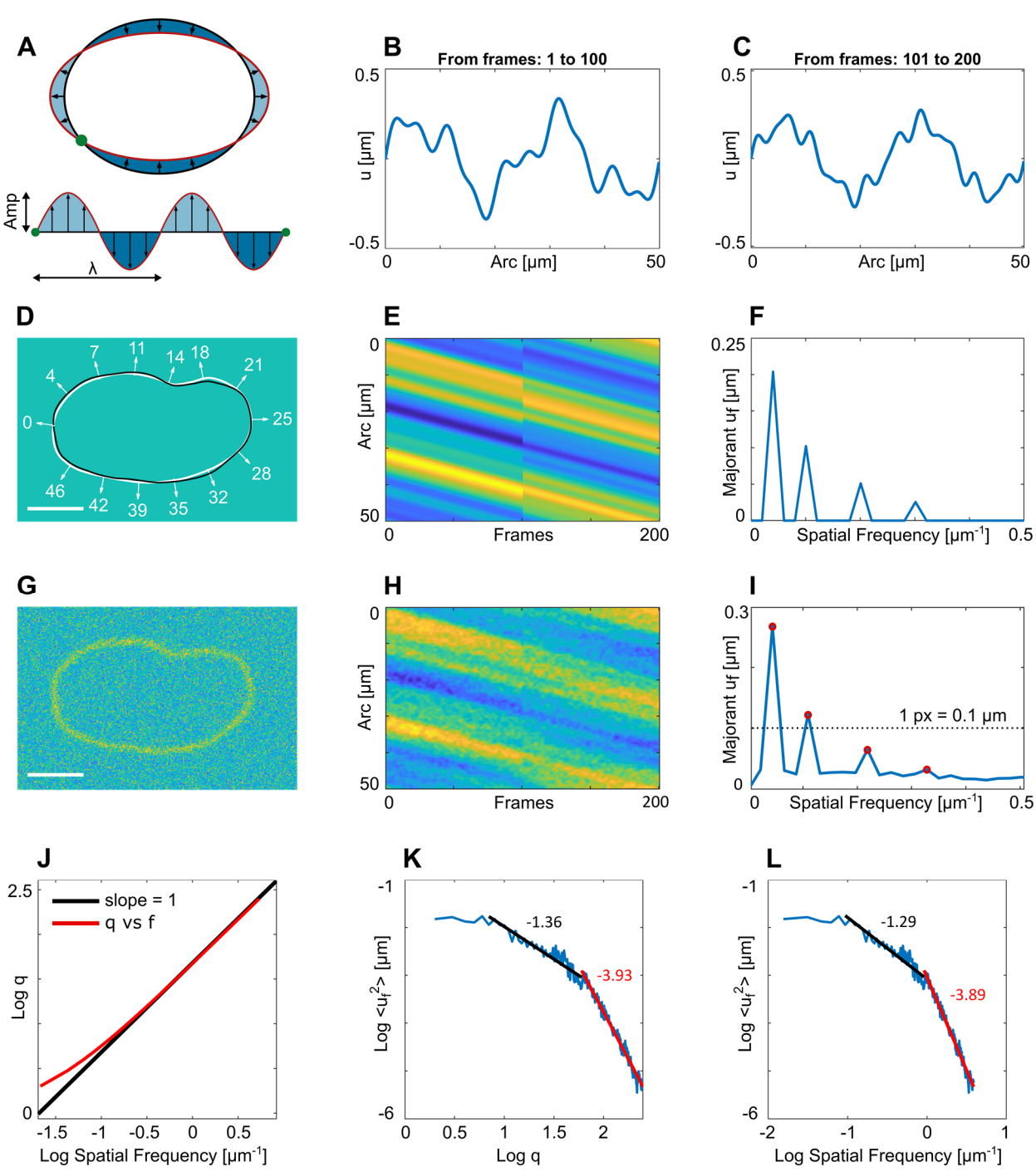

Figure S4. Validation of the membrane fluctuations. (A-I) Validation of the fluctuations values using synthetic videos. (A) Unfolding the distance between the current membrane (red) and the reference membrane (black) generates a waving signal (bottom) with characteristic wavelengths. For the compression fluctuation represented here, the associated unfolded fluctuations have a wavelength (λ) of half perimeter. (B) Unfolded fluctuation used between frames 1 and 100 to create the synthetic validation video. The full synthetic video has a total of four sinusoidal components: f_1 = 0.05 µm^{-1}, Amp_1 = 0.2 µm; f_2 = 0.1 µm^{-1}, Amp_2 = 0.1 µm; f_3 = 0.2 µm^{-1}, Amp_3 = 0.05 µm; f_4 = 0.3 µm^{-1}, Amp_4 = 0.025 µm. The fluctuations created between frames 1 and 100

have the components: {f_1, Amp_1}, {f_2, Amp_2} and {f_3, Amp_3}. (C) Unfolded fluctuation used between frames 101 and 200. The signal has three sinusoidal components: {f_1, Amp_1}, {f_3, Amp_3} and {f_4, Amp_4}. (D) First frame of synthetic membrane (black), waving around the reference membrane (white). Each frame was created by adding the associated fluctuation values to the reference membrane, along the direction of the normal vectors. Scale-bar: 5 µm. E) Expected fluctuation map of the entire video. The fluctuations (B and C) added to the reference membrane were continuously propagating around the nucleus in order to create a dynamic membrane. This generates the descending pattern shown in E. (F) Majorant of frequency depend fluctuations, u_f, obtained for the map E. The peaks of this curve reveal the amplitude and wavelengths of all the sinusoidal waves used to create the fluctuations. (G) First frame of the final synthetic video. Each frame was created by mapping the raw synthetic membranes (as shown in D) into a grid of pixels (1 px = 0.1 µm), followed by the addition of random noise. Scale-bar: 5 Scaler-bar: 5 µm. (H) Fluctuations map obtained by analyzing the noisy video G with Trackosome. The map is very similar to the expected result E, clearly showing the two different fluctuation patterns (before and after frame 100). (I) Majorant u_f obtained with Trackosome for the noisy video G, revealing the four expected peaks: $f_1^* = 0.044$ µm^{-1}, $Amp_1^* = 0.26$ µm; $f_2^* = 0.11$ µm^{-1}, $Amp_2^* = 0.12$ µm; $\lambda_3^* = 0.22$ µm^{-1}, $Amp_3^* = 0.065$ µm; $\lambda_4^* = 0.33$ µm^{-1}, $Amp_4^* = 0.032$ µm. Trackosome is able to detect fluctuations with amplitudes at the subpixel level in a highly noise environment. (J-K) Equivalence between slopes using wavenumber (q) and spatial frequency. (J) In logarithmic scales, q and spatial frequency are equivalent for frequencies above 0.1 µm^{-1}, making the slope analysis viable for the considered range. (K) Representative example of the average FT of the squared fluctuations, $\langle u_q^2 \rangle$, for a given cell, plotted against q, and the slopes of the linear fits (solid lines) at low and high frequencies. (L) Same $\langle u_f^2 \rangle$ curve as in B, but plotted against the associated spatial frequency. The slopes of the linear fits are very similar to those obtained in B.

References

Douglas Schwarz (2020). uipickfiles: uigetfile on steroids (https://www.mathworks.com/matlabcentral/fileexchange/10867-uipickfiles-uigetfile-on-steroids), MATLAB Central File Exchange. Retrieved October 15, 2020.